# Reversible high capacity nanocomposite anodes of Si/C/SWNTs for rechargeable Li-ion batteries

Wei Wang [a], Prashant N. Kumta [a,b,∗]

[a] *Department of Materials Science and Engineering, Carnegie Mellon University, Pittsburgh, PA 15213, USA*
[b] *Department of Biomedical Engineering, Carnegie Mellon University, Pittsburgh, PA 15213, USA*

## Abstract

Nanocomposites comprising silicon (Si), graphite (C) and single-walled carbon nanotubes (SWNTs), denoted as Si/C/SWNTs, have been synthesized by dispersing SWNTs via high power ultrasonication into a pre-milled Si/C composite mixture, followed by subsequent thermal treatment. The Si/C composite powder was prepared by high-energy mechanical milling (HEMM) of elemental Si and graphite using polymethacrylonitrile (PMAN) as a diffusion barrier suppressing the possible mechanochemical reaction between silicon and graphite to form SiC, and further prevent the amorphization of graphite during extended milling. A nanocomposite with nominal composition of Si-35 wt.% SWNTs-37 wt.% exhibits a reversible discharge capacity of ∼900 mAh g$^{-1}$ with an excellent capacity retention of capacity loss of 0.3% per cycle up to 30 cycles. Functionalization of the SWNTs with LiOH significantly improves the cyclability of the nanocomposite containing Si-45 wt.% SWNTs-28 wt.% exhibiting a reversible capacity of 1066 mAh g$^{-1}$ and displaying almost no fade in capacity up to 30 cycles. The improved electrochemical performance is hypothesized to be attributed to the formation of a nanoscale conductive network by the dispersed SWNTs which leads to successful maintenance of good electrical contact between the electrochemically active particles during cycling.
© 2007 Elsevier B.V. All rights reserved.

*Keywords:* Carbon nanotube; Anode; Lithium-ion; Mechanical milling

## 1. Introduction

Sony commercialized the first rechargeable lithium-ion (Li-ion) battery in 1991 [1] and since then lithium ion batteries have become the state-of-the-art rechargeable compact energy storage systems for portable consumer and industrial electronic devices. Due to their high energy density and flexible design, Li-ion batteries have been widely used as portable power sources for consumer electronics, computing, and telecommunication electronic devices. Graphite is currently used as the preferred commercial anode (negative electrode) material of choice in Li-ion batteries, which provides a theoretical capacity of 372 mAh g$^{-1}$. However, the tremendous progress made in the design of large-scale integrated circuits has provided the necessary impetus for miniaturization of electronic circuits and

devices. Consequently, there is a need for significant advances to be made in the design and engineering of lithium ion battery components to match the energy needs of modern computing and electronic devices. There is therefore a considerable need for safe, compact, light weight, higher energy density and longer lasting rechargeable batteries. These stringent requirements make it necessary to identify and design alternate anode materials.

Silicon is one of the most attractive and widely investigated candidate anode material due to its high theoretical specific capacity of 4200 mAh g$^{-1}$ corresponding to the fully lithiated composition of Li$_{4.4}$Si which is 10-fold higher than that of graphite [2–4]. However, there are severe crystallographic volume changes and several phase transitions occurring during the lithium alloying and de-alloying process. The mechanical strain generated in the process leads to cracking and crumbling of the electrode which results in the failure of the anode in a few cycles due to loss of electronic contact between the active particles [5].

In an attempt to improve the cyclability of the silicon-based anode, second phase components have been introduced to act

---

∗ Corresponding author at: Department of Materials Science and Engineering, Biomedical Engineering Carnegie Mellon University, Pittsburgh, PA 15213, USA.

*E-mail address:* kumta@cmu.edu (P.N. Kumta).

as a buffering matrix to accommodate the large volume change upon cycling. Among the different matrix materials considered, graphite is a good candidate due to its good electronic conductivity and lubrication characteristics. Si/C composites have therefore attracted considerable interest and the electrochemical performance reported so far appear quite promising. In recent years, different particle sizes, crystallographic variations of silicon and carbon have been used as the starting materials to synthesize Si/C composites. These include variants of nanocrystalline and amorphous silicon, graphite, MCMB and disordered carbon [6–19]. Several strategies, such as decomposition of organic precursors [6–10], high energy mechanical milling (HEMM) [11–15], physical mixing [16,17], and carbon coating on silicon particles [18,19] have also been implemented by a number of groups. Recently, Datta et al. demonstrated a composite exhibiting a reversible capacity of ∼660 mAh g$^{-1}$ and excellent capacity retention by using silicon, graphite and polyacrylonitrile-based disordered carbon generated by high energy mechanical milling, followed by subsequent heat-treatment [15]. Despite these advances made, the generation of an anode exhibiting a stable reversible capacity of above 1000 mAh g$^{-1}$ still appears to be a challenge. There is still therefore a need to identify alternative matrix systems that can accommodate the large volumetric stresses generated by lithiation and de-lithiation of silicon to provide a stable, reversible discharge capacity.

Carbon nanotubes (CNTs) have received considerable interest as Li insertion host materials since their discovery in 1991 [20]. Although CNTs in general, as reported in the literature are known to exhibit a higher reversible capacity than graphite [21–27], a high irreversible loss and a large voltage hysteresis are commonly observed in the cycling performances of CNTs, which greatly limit their use as an anode material in Li-ion batteries. Nevertheless, CNTs prove to be a better choice over graphite as a matrix material for Li-ion anodes due to their excellent physical properties including superior mechanical strength (Young's modulus ∼1.0 TPa) [28] and electrical conductivity (resistivity <10$^{-4}$ Ω cm) [29] in comparison to any of the existing materials systems known to date. They also possess some unparalleled properties such as a large aspect ratio, structural flexibility, and tortuosity [30]. Exploitation of these unique attributes of CNTs combined with its nanoscale dimensions will enable the generation of a nanoscale conductive network which can potentially improve the electrical contact between the active silicon particles. As a result, the structural integrity of the anode during cycling can be maintained, thus making it a candidate matrix material.

Chen et al. and Guo et al. were the first two groups to report the utilization of multi-walled carbon nanotubes (MWNTs) as host materials to generate Sb and SnSb$_{0.5}$-MWNTs nanocomposites by a chemical reduction method [31,32]. Although the cyclability is improved compared to the pure metal anode, both systems suffer from a relatively high capacity fade of >1.1% per cycle. More recently, Ishihara et al. reported a carbon nanotube coating of Cr doped silicon anode generated by chemical vapor deposition (CVD) technique which demonstrated a reversible capacity of 1250 mAh g$^{-1}$ for 10 cycles [33]. Shu et al. also

Table 1
Comparison of the physical properties of MWNTs and SWNTs

| | Diameter (nm) | Young's modulus (GPa) | Specific surface area (m$^2$ g$^{-1}$) |
|---|---|---|---|
| MWNTs | 3–30 | 1800 [37] | ∼500 |
| SWNTs | 1–2 | 1280 [38] | 1315 [39] |

reported a nanotubes/Si composite synthesized by growing the carbon nanotubes on superfine silicon particles via CVD method [34]. MWNTs/Si nanocomposites were also prepared through high energy mechanical milling (HEMM) by both Zhang et al. [35] and Eom et al. [36], which exhibited a high first cycle discharge capacity (>2000 mAh g$^{-1}$), but unfortunately displayed poor capacity retention.

Although different methods have been successfully used to synthesize the MWNTs/Si nanocomposite, the capacity retention of the reported anode materials is still limited thus preventing its use for commercial application. This is possibly due to the inhomogeneous distribution of silicon particles within the CNTs. Moreover, single-walled carbon nanotubes (SWNTs) which exhibit a more perfect structure than MWNTs due to the presence of reduced number of defects has not yet been studied to date as the host matrix to the best of our knowledge. Table 1 shows a comparison of the properties of MWNTs and SWNTs. The SWNTs are expected to form a nanoscale conductive network connecting several contact points with the electrochemically active Si. Furthermore, they are expected to exhibit better overall mechanical stiffness because of their smaller dimensions, higher specific surface area, and better mechanical strength compared to MWNTs thus rendering them as excellent candidate matrices for containing the electrochemically active Si phase. In this study, high power sonication is employed to disperse the SWNTs into the pre-milled Si/C powder to generate the Si/C/SWNTs nanocomposites for use as Li-ion anode materials. The charge/discharge performance corresponding to the insertion/extraction of Li ions into/from the Si/C/SWNTs nanocomposite is also analyzed using various electrochemical characterization methods.

## 2. Experimental

0.84 g Polymethacrylonitrile (PMAN) (Scientific Polymer Product) was dissolved in ∼10 mL N-methylpyrrolidinone (NMP) to form a homogeneous solution. Mixtures of elemental powders of graphite (∼0.3 g, Aldrich, 1–2 μm), Si (∼0.54 g Alfa Aesar, −325 mesh), and PMAN solution were loaded into a SS vial containing 10 mm diameter SS balls with a charge ratio of 20:1 inside an argon filled glove box (VAC Atmospheres, Hawthorn, CA, ∼10 ppm oxygen and ∼0.10 ppm moisture) in order to prevent and minimize any oxidation of the starting materials. The PMAN solution covers the starting precursors and the milling media completely inside the vial, which was helpful to prevent excessive cold welding, agglomeration and temperature build up during the first high energy milling process. Mixtures of graphite, silicon, and PMAN solution were subjected to mechanical milling up to 15 h using a SPEX Cer-

tiPrep 8000M high-energy mechanical mill, and then dried in a vacuum oven at 383 K overnight. The mechanically milled powders and SWNTs (~0.8–1.2 nm in diameter, ~100–1000 nm in length, Carbon Nanotechnologies, Inc., Houston, TX) were dispersed simultaneously in a toluene solution for 15 min using a high power ultrasonicator (Misonix-300, Farmingdale, NY) operating at a power level of 20 W. The solution was then filtered and the powder was dried in an environmental oven at 358 K overnight. In order to decompose PMAN, the powders were annealed isothermally at 1073 K for 6 h in an ultra high purify argon (UHP-Ar) gas using a heating rate of 10 K min$^{-1}$ and a flow rate of 100 mL min$^{-1}$. The powder was hand ground before the preparation of the electrode for electrochemical testing.

In order to identify the decomposition temperature and the yield of PMAN, thermo gravimetric analysis (TGA) has been performed for pure PMAN under UHP-Ar in a TGA machine (TA 2960, TA Instrument, New Castle, DE) utilizing ~7 mg PMAN and employing a heating rate of 10 K min$^{-1}$. The milled as well as the heat treated powders were characterized by X-ray diffraction (XRD) using Philips XPERT PRO system with Cu Kα (λ = 0.15406 nm) radiation in order to identify the phases present. Scanning electron microscopy (SEM) (Philips XL30 operating at 20 kV) was employed to investigate the microstructure of the as prepared composites as well as the electrochemically cycled samples. High-resolution transmission electron microscopy (HRTEM, Philips Tecnai 20 FEG) was also used to observe the morphology, structure and particle size of the as-prepared nanocomposite powders. For HRTEM analysis, the Si/C/SWNTs powders were dispersed on 3.05 mm diameter copper grids (electron microscopy science) containing a holey carbon film in methanol by sonication followed by drying under vacuum for 24 h. Fourier transform infrared spectroscopy (FTIR) was performed on the samples before cycling and after 30 cycles, which had been washed with dimethyl carbonate (DMC) inside the UHP-Ar glove box for 24 h to remove the presence of any remaining lithium containing electrolyte in the electrodes. They were then dried in a vacuum oven at 90 °C for 24 h to remove any excess solvent. The samples were mixed with KBr in a ratio of 1:100, respectively. A pellet was prepared by pressing the dried, milled sample to 3000 psi for 2 min using a Carver 10 ton hand operated press. A Mattson Galaxy Series FTIR 5000 in transmission mode was used to collect the spectra in the scan range of 400–4000 cm$^{-1}$.

The Si/C/SWNTs nanocomposite electrodes were fabricated on copper substrate of approximately 10 mm diameter in order to evaluate the electrochemical characteristics primarily involving constant current cycling tests. 82 wt.% of the active powder, 8 wt.% acetylene carbon black and 10 wt.% of polyvinylidene fluoride (PVDF) binder dissolved in *N*-methylpyrrolidinone (NMP) were mixed to produce a slurry which was then coated onto a copper foil and dried over night at 383 K in a vacuum oven prior to assembling the customized test cell. The active materials loading on the anode is around 2 mg on a 1 cm$^2$ current collector area. A prototype hockey puck cell design was utilized for the electrochemical tests employing a lithium foil as the counter electrode and 1 M LiPF$_6$ in ethylene carbonate (EC)/dimethyl carbonate (DMC) (2:1) as the electrolyte. All the batteries tested

in this study were cycled from 0.02 to 1.2 V employing a constant current density of 250 μA cm$^{-2}$ and a minute rest period between the charge/discharge cycles using a potentiostat (Arbin electrochemical instrument).

## 3. Results and discussion

It is known that achieving a more homogeneous distribution of the active silicon particles in the graphite matrix is critical for improving the capacity retention of the composite leading to enhanced cycle life in the case of the Si/C composite anode. Therefore, high-energy mechanical milling (HEMM) has been used widely to generate Si/C based composites [11,12]. Extended milling however has been shown to result in the formation of SiC which lowers the capacity due to consumption of the active element. For HEMM to be useful for generating Si/C based composites exhibiting highly reversible stable capacity, the mechanochemical reaction between silicon and carbon which results in the formation of SiC and the amorphization of graphite during extended milling must be substantially suppressed. One approach to prevent the reaction between Si and C is the use of polymer additives that can be decomposed at low enough temperatures following pyrolysis after milling with much reduced yield of carbon.

Different polymers have been used as milling additives to act as diffusion barriers between Si and graphite to circumvent the formation of SiC as reported previously [13–15]. In this study, extended mechanical milling of Si and graphite has been conducted in the presence of PMAN used as the polymer additive mainly to achieve the above goal. In order to identify the decomposition temperature and weight loss of PMAN, thermogravimetric (TGA) analysis has been performed on pure PMAN. The TGA result of PMAN, shown in Fig. 1, exhibits a typical decomposition behavior of the polymer with complete decomposition occurring at a temperature of 673 K resulting in a very low yield of carbon residue of ~4% after pyrolysis. A low carbon residue is preferred for improved electrode performance, since most of the carbon generated after high temperature treatment is largely amorphous and non conducting contributing to a significantly large irreversible loss due to the formation of the
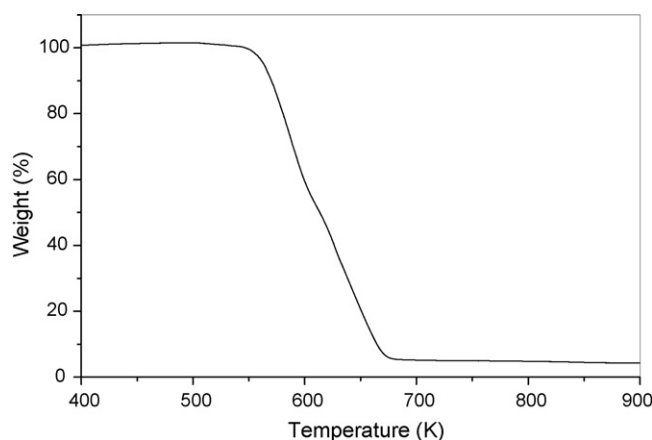


Fig. 1. TGA analysis of pure PMAN conducted in ultra high purity Argon.

solid electrolyte interphase (SEI) layers. Based on thermal analysis, the resultant milled composites were thermally treated at 1073 K for 6 h in UHP-Ar to completely decompose the PMAN polymer additive.

Two different compositions of Si/C/CNTs samples were studied in the present work. The first contains approximately 35 wt.% Si, 37 wt.% SWNTs and 27 wt.% graphite with the balance 1 wt.% of residual carbon arising from the thermal decomposition of PMAN (PMAN-C), thereafter denoted as 35Si-37SWNTs. The second sample contains approximately 45 wt.% Si, 28 wt.% SWNTs and 26 wt.% graphite with the residual of 1 wt.% of C arising from PMAN-C, thereafter denoted as 45Si-28SWNTs. These two compositions were synthesized by dispersing SWNTs into the pre-milled Si/C powder in the presence of toluene by high power ultrasonication for 15 min at a power level of 20 W. The Si/C powder was pre-milled for 15 h before mixing with the SWNTs. The resultant composite was then subjected to heat treatment at a temperature of 1073 K in UHP-Ar for 6 h. Fig. 2 shows the XRD pattern of the silicon and graphite powder obtained after 15 h of ball milling and the 35Si-37SWNTs sample after mixing the pre-milled Si/C powders with SWNTs followed by heat treatment. These two spectra are nearly identical, which demonstrate only the presence of silicon and graphite without any detectable amount of SiC formed as a result of milling. The presence of graphite revealed in the XRD pattern (Fig. 2(a)) also suggests that with the addition of PMAN, the crystal structure of graphite is well preserved even after 15 h of milling. Compared with dry milling of Si and graphite as reported by us before [13] the amorphization of graphite is considerably reduced. A similar XRD pattern is also exhibited by the 45Si-28SWNTs sample, which is not shown here due to space limitations.

The variation of specific gravimetric capacity with cycle number of the 35Si-37SWNTs nanocomposite is shown in Fig. 3. Electrochemical tests were not conducted on pure SWNTs due to the cost and limited supply of these nanotubes of the desired purity. A reversible capacity of 460 mAh g$^{-1}$ reported by Claye et al. [25], the same group that produced the SWNTs
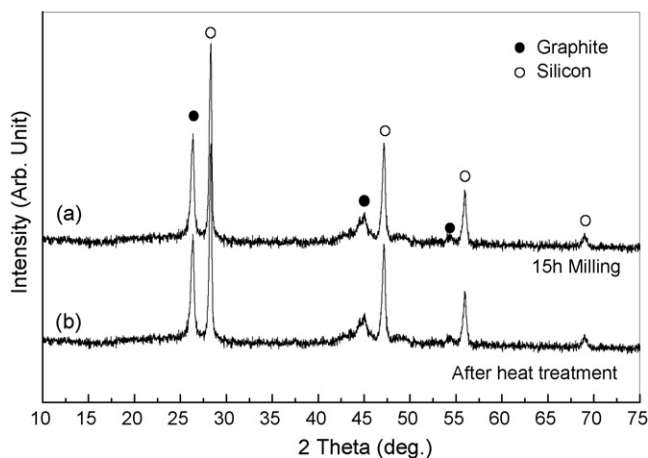


Fig. 2. (a) XRD pattern of Si/C composite powder after 15 h milling. (b) XRD pattern of 35Si-37SWNTs nanocomposite after mixing with SWNTs followed by heat treatment at 1073 K for 6 h in UHP-Ar.
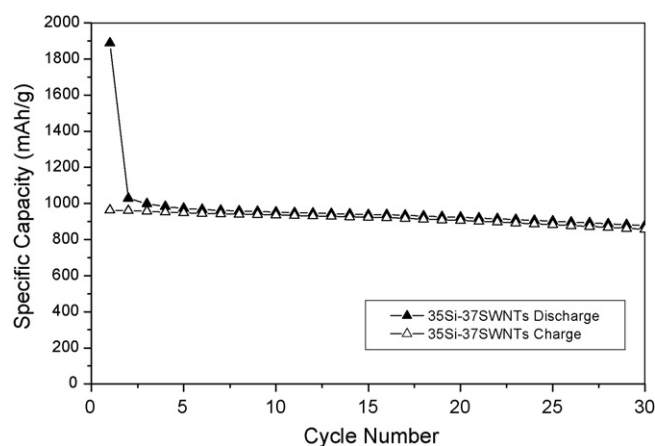


Fig. 3. Variation of specific capacity with cycle number of 35Si-37SWNTs nanocomposite sample electrode cycled at a rate of 250 μA cm$^{-2}$.

tested in this study, was however used to calculate the theoretical capacity of the composites. The calculations yield a capacity of ∼1125 mAh g$^{-1}$ for the sample corresponding to 35Si-37SWNTs, in which Si, SWNTs and graphite contribute approximately 70%, 20% and 10% of the capacity, respectively, and carbon from the thermal decomposition of PMAN is neglected due to the very low yield (∼4%) of carbon residue. The 35Si-37SWNTs nanocomposite exhibits a 1st discharge and 1st charge capacity of ∼1882 and ∼960 mAh g$^{-1}$, respectively, with a capacity loss of 0.3% per cycle up to 30 cycles. The 1st charge capacity is close to the calculated theoretical capacity. However the loss of ∼165 mAh g$^{-1}$ could arise from several factors such as residual oxide catalyst particles remaining in the SWNTs following purification of the nanotubes as well as possible oxidation of silicon during HEMM and subsequent heat treatment. Although there was no presence of any iron silicide detected in the XRD analysis of the HEMM derived Si/C powders, it is possible that there could be some iron contamination from the steel vial and milling media that could reduce the active silicon lowering the capacity. The 35Si-37SWNTs nanocomposite demonstrates an irreversible capacity loss of 49%, which is higher than that of the Si/C composites reported by Datta and Kumta [15]. A Si/C composite comprising 35 wt.% Si and 64 wt.% graphite with balance PMAN decomposed carbon has been prepared and tested using the same experimental method, which exhibits a 1st discharge and 1st charge capacity of ∼1365 and ∼977 mAh g$^{-1}$, respectively, and hence yields an irreversible loss of 28% equivalent to a Coulombic efficiency of 72%. Therefore, compared with the Si/C composite containing identical amounts of silicon, the much higher irreversible loss of 49% for 35Si-37SWNTs sample can be attributed to SWNTs which contributes approximately 517 mAh g$^{-1}$ of irreversible capacity.

The irreversible capacity usually originates from the formation of SEI layers due to the redox reaction of Li$^+$ with the electrolyte solvent molecules. The SEI formation has been correlated with the surface area in the carbon anode by Tarascon's group [40] and it is reasonable to believe that the same mechanism would apply to the SWNTs in the present case. The Brunauer–Emmett–Teller (BET) specific surface area of the
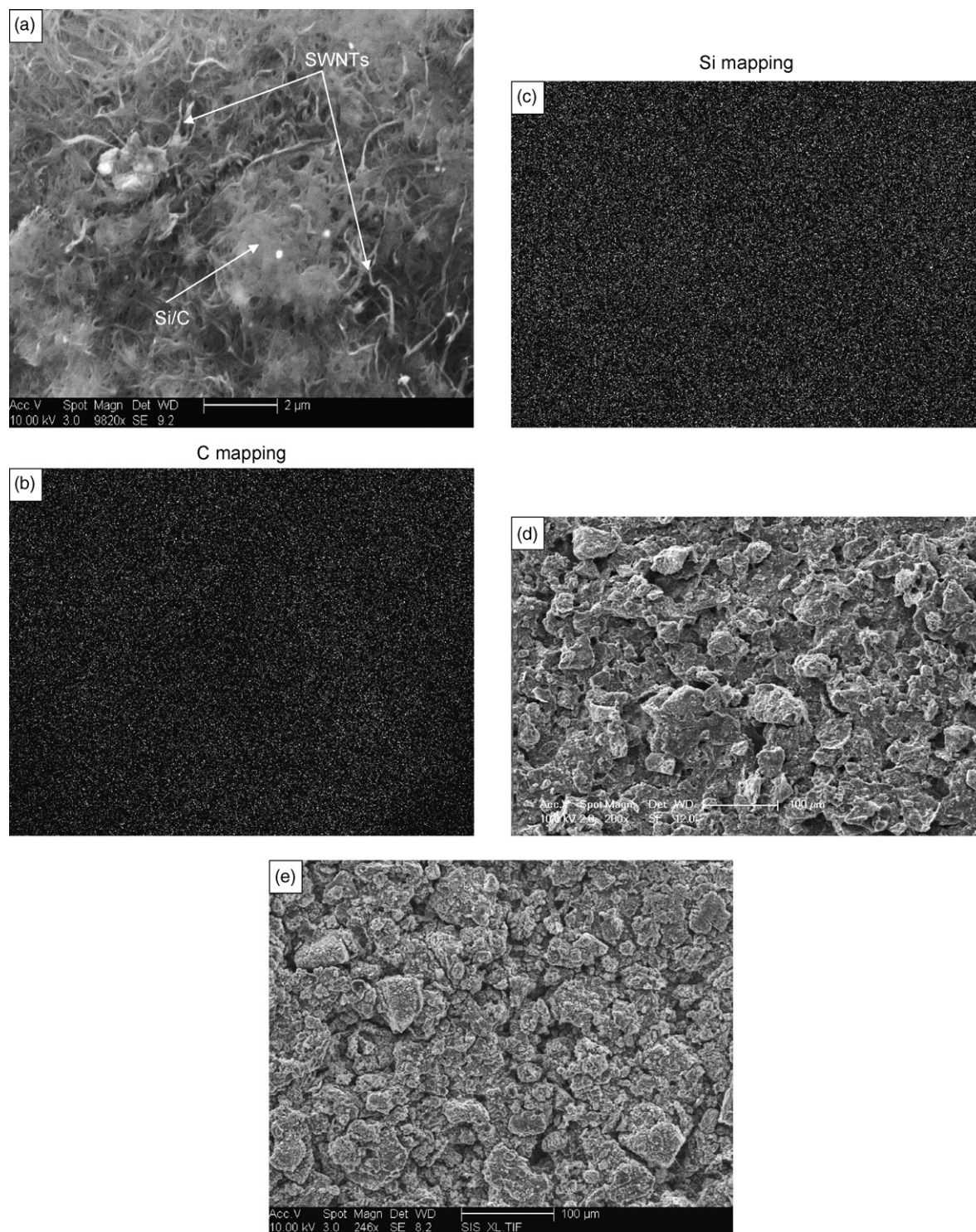
Fig. 4. (a) SEM micrograph of 35Si-37SWNTs nanocomposite sample, (b) chemical map of C, and (c) chemical map of Si, respectively, using EDX. All images are taken at the same scale as shown in (a). (d) SEM micrograph of the as prepared electrode and (e) the electrode after 30 cycles.

SWNTs used in this study is ~400–100 m$^2$ g$^{-1}$ as measured by the supplier, which is much larger than that of graphite, and consequently could be expected to contribute to a larger irreversible capacity. It is also reported that the purification treatment which employs strong oxidizing acid can partially functionalize the carbon nanotubes resulting in the formation of oxygenated functional groups [41]. The reduction of these oxygenated species

also contributes to the irreversible capacity. The presence of oxygenated species on the surface of the carbon nanotubes has been confirmed by Frackowiak et al. by XPS analysis [42]. The large irreversible loss of CNTs upon cycling has also been reported by several researchers as discussed before [25–27].

The SEM images of the prepared nanocomposite electrode are shown in Fig. 4. As can be seen from Fig. 4(a), the dense
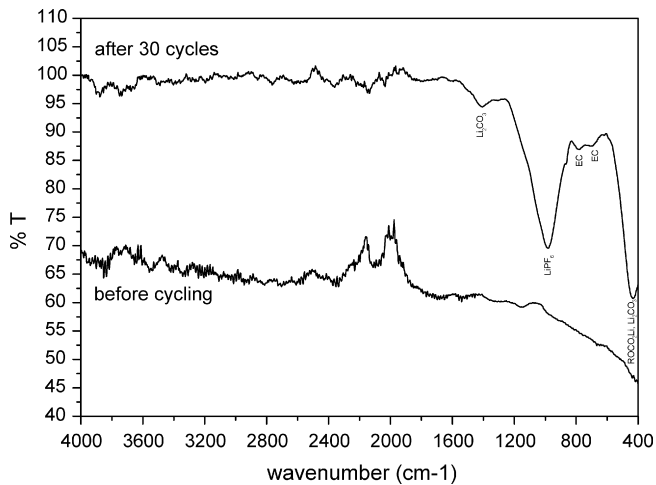
Fig. 5. FTIR plots for 35Si-37SWNTs nanocomposite before and after 30 cycles.

SWNTs films appear to wrap around the graphite particles while also encapsulating the silicon particles. EDX mapping of the different elements was conducted to analyze the distribution of the different phases presented in the nanocomposite, which is shown in Fig. 4(b and c), respectively. As revealed in the EDX elemental maps, both silicon and carbon are homogeneously distributed within the nanocomposite.

The SEM analysis was also conducted on the electrodes before and after cycling samples in order to investigate any change in the microstructure or morphology of the particles during the alloying and de-alloying processes. Fig. 4(d and e) shows the morphologies of the uncycled and cycled samples of the Si/C/SWNTs electrodes fabricated from the nanocomposite corresponding to the composition, 35Si-37SWNTs. The surface of the electrode after 30 cycles is devoid of any cracks, which indicates the excellent structural integrity even after 30 cycles. There also appears to be no significant change in the overall morphology of the particles before and after cycling. However, there appears to be indication of evolution of a fine structure on the surface of the particles, probably corresponding to a surface reaction with the electrolyte and formation of the SEI layer. When a liquid electrolyte consisting of 1 M LiPF$_6$ in ethylene carbonate/dimethyl carbonate is used with a graphite anode, the SEI layer is mainly comprised of LiF, Li$_2$CO$_3$ and some Li$_2$O [43]. Fig. 5 shows the FTIR spectra conducted on the electrode before and after the electrochemical cycling of the 35Si-37SWNTs nanocomposite. Compared with the published work on similar systems containing graphite anode, it can be seen that alkyl lithium carbonates ROCO$_2$Li, lithium carbonate, Li$_2$CO$_3$, and ethylene carbonate were found to be present in the electrode cycled after 30 cycles [43]. Apart from the presence of the SEI products contributing to the fine sub structure on the surface of the particles, it appears that the electrode microstructure and the overall structure are indeed preserved. The overall microstructural and structural integrity of the electrode is probably responsible for the good stability and cyclability of the SWNTs containing composites.

Compared with the capacity of ∼650 mAh g$^{-1}$ for Si/C composites reported in the literature [15], the incorporation of the SWNTs into the Si/C composite results in a nanocomposite anode material with high reversible capacity and excellent capacity retention. This significant improvement in the cyclic performance for Si/C/SWNTs system is attributed to the maintenance of the electronic contact during cycling through the secondary nanosized conductive matrix formed by the SWNTs. During extended milling the silicon particles are homogeneously dispersed and embedded into the more ductile graphite matrix which forms the first intra-type composite matrix to accommodate the volume change of the silicon particles during alloying and de-alloying with lithium upon cycling as reported by Datta et al. [44]. However, in an attempt to increase the silicon content to increase the reversible capacity, the graphite matrix alone is not sufficient enough to accommodate the large volume change of silicon, which leads to the cracking and crumbling of the Si/C particles thus forming finer particles. The loss in electronic contact with the finer Si particles therefore results in the gradual degradation of the electrode. However, it is possible that SWNTs that have been homogeneously dispersed in the Si/C mixture form a secondary nanoscale conductive matrix due to the ability of the SWNTs to bend around the Si/C particles, thus wrapping the particles, holding them together and preserving the electronic contact. With the formation of the secondary nanosized conductive matrix, these finer particles are kept in contact within this matrix and thus the integrity of the electrode is largely maintained, which leads to a significantly improved electrochemical cycling performance. The proposed hypothesis is illustrated by the schematic in Fig. 6.

To verify the formation of the secondary nanosized conductive matrix by SWNTs, HRTEM analysis was conducted on the 35Si-37SWNTs nanocomposite obtained after heat-treatment,
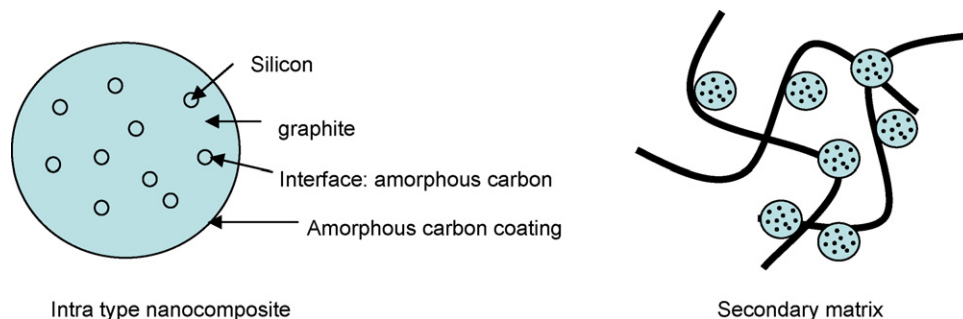


Fig. 6. Schematic illustration of the proposed concept of intra and secondary matrix type Si/C/SWNTs nanocomposite.
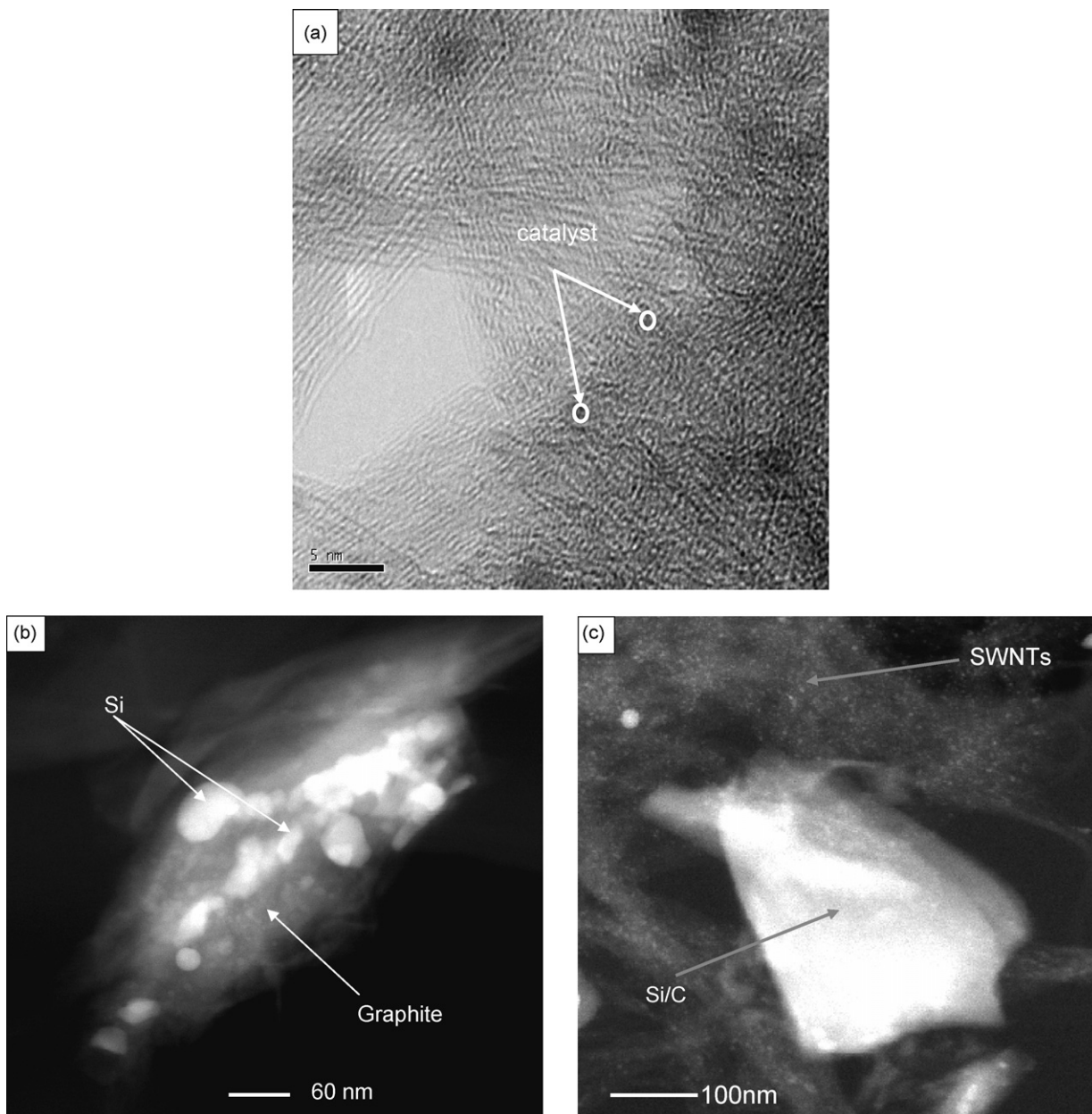
Fig. 7. (a) Network formed by SWNTs. (b) Si embedded in the graphite particle. (c) Si/C particles residing within the SWNTs network for 35Si-37SWNTs nanocomposite.

the results of which are shown in Fig. 7. The HRTEM micrograph of SWNTs in the Si/C/SWNTs sample is shown in Fig. 7(a), which reveals the network formed by clusters of SWNTs. The dark spherical particles ∼3 nm in Fig. 7(a) correspond to the catalyst particles used to generate the SWNTs. The HRTEM micrograph of silicon (∼10–30 nm) embedded in the carbon matrix during extended milling of 15 h is shown in Fig. 7(b). Fig. 7(c) shows the Si/C particles residing in the network formed by SWNTs. The HRTEM results described above clearly show that the milled Si/C particle composite is contained within the nanoscale network created by the SWNTs. The narrow aspect ratio of the SWNTs combined with their ability to bend thus helps to preserve the connectivity between the Si/C particles. Therefore, the active Si particles can undergo alloying and

de-alloying with lithium without losing electrical contact with carbon and the fragmented silicon particles. This structural integrity helps the composite to exhibit the excellent capacity and stability.

The plot of differential capacity with cell potential for the nanocomposite sample of 35Si-37SWNTs is shown in Fig. 8. Upon examination of the differential capacity plot of the nanocomposite, peaks can be observed at ∼0.22, 0.15, 0.10 and 0.07 V corresponding to the reaction of Li-ions with graphite [45]. The appearance of the peaks at ∼0.09, ∼0.24 and ∼0.29 V after the first cycle is characteristic of the alloying reaction of lithium with silicon. The appearance of these peaks also suggests the conversion of crystalline silicon to an amorphous state after the first cycle. Claye and Gao reported the appearance of
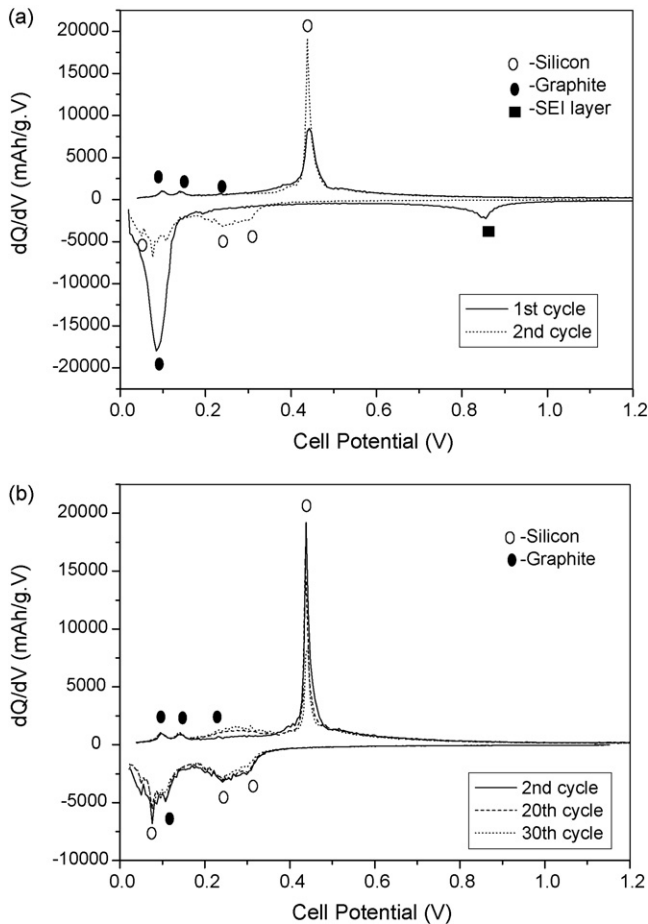
Fig. 8. Plots of differential capacity with cell potential for 35Si-37SWNTs nanocomposite electrode. (a) After 1st and 2nd cycle and (b) after 2nd, 20th and 30th cycle.
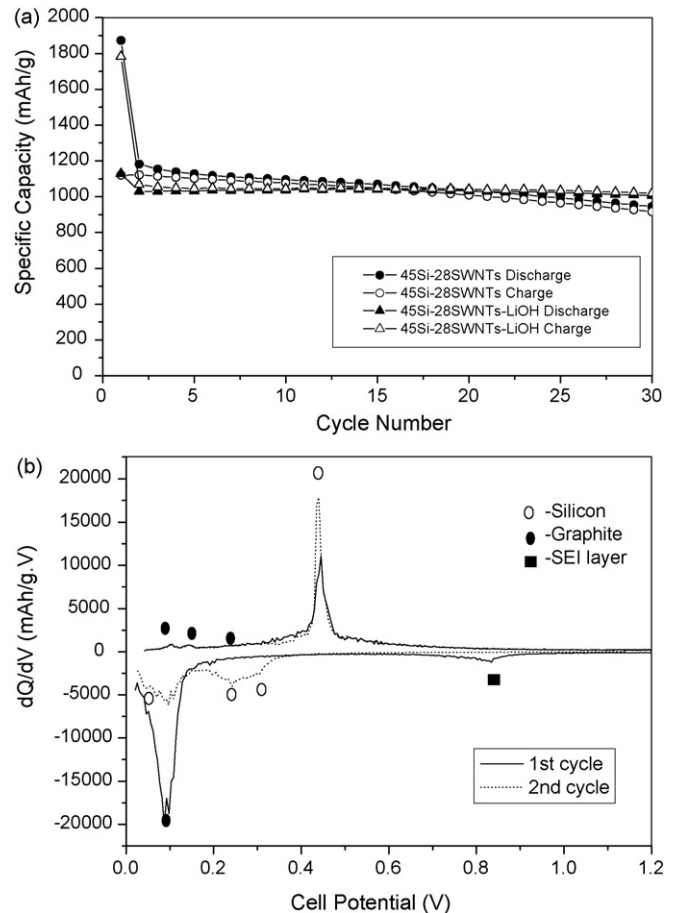


Fig. 9. (a) Comparison of specific capacity with cycle number of 45Si-28SWNTs nanocomposite electrode with and without LiOH, both cycled at a rate of $250\,\mu A\,cm^{-2}$. (b) Plot of differential capacity with cell potential of the 45Si-28SWNTs sample functionalized with LiOH.

a voltage plateau on the first cycle of voltage-capacity plot of SWNTs at 0.75 and 0.9 V, respectively [25,26]. This plateau does not occur in the subsequent cycles and is attributed to the formation of SEI. Similarly, in this study, the formation of a SEI layer is identified by the presence of a broad peak at ~0.85 V in Fig. 8. The mechanism for Li ions insertion in SWNTs is not fully understood yet. However, there are no obvious peaks corresponding to insertion/extraction of the lithium ions into/from the SWNTs seen in Fig. 8, which suggests that unlike the staging mechanism observed in graphite there is no well-defined redox potential for lithium insertion or extraction with the SWNTs. There are also no reports thus far on the insertion reaction of Li with SWNTs.

In an attempt to improve the cycling stability of the sample 45Si-28SWNTs, LiOH has been added into the system by sonicating it with SWNTs prior to mixing with Si/C powders with a 1:1 atomic ratio corresponding to SWNTs in methanol via ultrasonication. The solution was then filtered and the collected powder was dried and mixed with Si/C powder as described before. The cycling stability has been significantly improved as shown in Fig. 9. Without the functionalization of the SWNTs with LiOH, the 45Si-28SWNTs nanocomposite exhibits a 1st discharge and 1st charge capacity of ~1872

and ~1121 mAh g$^{-1}$, respectively, with a capacity loss of 0.6% per cycle up to 30 cycles. The loss in the reversible capacity compared with the calculated theoretical capacity of ~1370 mAh g$^{-1}$ could be attributed to the same reasons as discussed previously for 35Si-37SWNTs nanocomposite. A significantly lower irreversible loss of 40% however is observed for the 45Si-28SWNTs nanocomposite compared with that of 35Si-37SWNTs nanocomposite, which is due to the fact that 45Si-28SWNTs nanocomposite contains a lower (9%) amount of SWNTs and therefore the surface area contribution to SEI formation is correspondingly lower. This result is in well agreement with the previous discussion of the origin of the high irreversible loss in the Si/C/SWNTs nanocomposite. After the functionalization the capacity loss has significantly improved from 0.6% per cycle to almost no fade up to 30 cycles as shown in Fig. 9(a). The irreversible loss is also slightly decreased from 40% to 37%. The differential capacity with cell potential for the nanocomposite samples containing LiOH is also shown in Fig. 9(b), which is identical to Fig. 8. The improved stability could arise from the reaction of LiOH with silicon to form Li$_2$SiO$_3$ during heat treatment. This layer may enhance the interface strength between silicon and carbon, and also between silicon and SWNTs, which leads to a better cycling performance. Possible formation of

$Li_2SiO_3$ however consumes some silicon within the sample. Consequently the overall capacity of 1066 mAh/g upto 30 cycles is slightly lower than the sample containing no LiOH. More detailed study is currently under way to elaborate the exact role of the LiOH additive and validate the proposed hypothesis.

## 4. Conclusion

Si/C/SWNTs nanocomposites were successfully synthesized by dispersing SWNTs into the pre-milled Si/C powder using high power ultrasonication in toluene followed by a heat treatment at a temperature 1073 K for 6 h. A composite containing 35 wt.% of Si and 37 wt.% SWNTs exhibited a stable capacity of ~900 mAh g$^{-1}$ with moderate capacity retention of ~0.3% loss per cycle up to 30 cycles. The excellent capacity retention of Si/C/SWNTs with such a high reversible capacity is attributed to the formation of the nanosized conductive network matrix by SWNTs maintaining a good electrical contact between the silicon and graphite particles. The formation of the SEI layer due to the presence of the oxygenated species attached to the surface of the SWNTs contributes to the large irreversible loss of 49-37%. Functionalization of the SWNTs with LiOH improves the reversible capacity to 1066 mAh g$^{-1}$ up to 30 cycles with no measurable capacity loss. These results suggest that the Si/C/SWNTs nanocomposite is a very promising system for application as an alternative lithium-ion anode. The system clearly deserves further research and a systematic study is very much warranted.

## Acknowledgments

## References

[1] T. Nagaura, K. Tozawa, Prog. Batteries Solar Cells 9 (1990) 209.
[2] B.A. Boukamp, G.C. Lesha, R.A. Huggins, J. Electrochem. Soc. 128 (1981) 725.
[3] K. Amezawa, N. Yamamoto, Y. Tomii, Y. Lto, J. Electrochem. Soc. 145 (1998) 1986.
[4] W.J. Weydanz, M. Wohlfahrt-Mehrens, R.A. Huggins, J. Power Sources 81/82 (1999) 237–242.
[5] J.H. Ryu, J.W. Kim, Y.E. Sung, S.M. Oh, Electrochem. Solid-State Lett. 7 (2004) A306.
[6] A.M. Wilson, J.R. Dahn, J. Electrochem. Soc. 142 (2) (1995) 326.
[7] A.M. Wilson, W. Xing, G. Zank, B. Yates, J.R. Dahn, Solid State Ionics 100 (1997) 259.
[8] W. Xing, A.M. Wilson, G. Zank, J.R. Dahn, Solid State Ionics 93 (1997) 239.
[9] J. Yang, B.F. Wang, K. Wang, Y. Liu, J.Y. Xie, Z.S. Wen, Electrochem. Solid-State Lett. 6 (8) (2003) A154.
[10] Z.S. Wen, J. Yang, B.F. Wang, K. Wang, Y. Liu, Electrochem. Commun. 5 (2003) 165.
[11] C.S. Wang, G.T. Wu, X.B. Zhang, Z.F. Qi, W.Z. Li, J. Electrochem. Soc. 145 (8) (1998) 2751.
[12] G.X. Wang, J. Yao, H.K. Liu, Electrochem. Solid-State Lett. 7 (8) (2004) A250–A253.
[13] I. Kim, G.E. Blomgren, P.N. Kumta, J. Power Sources 130 (2004) 275.
[14] I. Kim, P.N. Kumta, J. Power Sources 136 (2004) 145.
[15] M.K. Datta, P.N. Kumta, J. Power Sources 158 (2006) 557.
[16] H. Li, X. Huang, L. Chen, Zh. Wu, Y. Liang, Electrochem. Solid-State Lett. 2 (11) (1999) 547–549.
[17] M. Holpzafel, H. Buqa, L.J. Hardwick, M. Hahn, A. Wursig, W. Scheifele, P. Novak, R. Kotz, C. Veit, F.-M. Petrat, Electrochim. Acta 52 (2006) 973.
[18] W.R. Liu, J.H. Wang, H.Ch. Wu, D.Ts. Shieh, M.H. Yang, N.L. Wu, J. Electrochem. Soc. 152 (2005) A1719.
[19] M. Yoshio, H. Wang, K. Fukuda, T. Umeno, N. Dimov, Z. Ogumi, J. Electrochem. Soc. 149 (2002) A1598.
[20] S. Iijima, Nature 354 (1991) 56.
[21] G. Maurin, Ch. Bousquet, F. Henn, P. Bernier, R. Almairac, B. Simon, Chem. Phys. Lett. 312 (1999) 14.
[22] G. Maurin, F. Henn, B. Simon, J.F. Colomer, J.B. Nagy, Nanoletters 1 (2001) 75.
[23] E. Frackowiak, S. Gautier, H. Gaucher, S. Bonnamy, F. Béguin, Carbon 37 (1999) 61.
[24] T. Ishihara, A. Kawahara, M. Nishigushi, M. Yoshio, Y. Takita, J. Power Sources 97/98 (2001) 129.
[25] A.S. Claye, J.E. Fischer, C.B. Huffmann, A.G. Rinzler, R.E. Smalley, J. Electrochem. Soc. 147 (2000) 2845.
[26] B. Gao, A. Kleinhammes, X.P. Tang, C. Bower, L. Fleming, Y. Wu, O. Zhou, Chem. Phys. Lett. 307 (1999) 153.
[27] H. Shimoda, B. Gao, X.P. Tang, A. Kleinhammes, L. Fleming, Y. Wu, O. Zhou, Phys. Rev. Lett. 88 (2002), 015502- 1.
[28] M.-F. Yu, B.S. Files, S. Arepalli, R.S. Ruoff, Phys. Rev. Lett. 84 (2000) 5552.
[29] A. Thess, R. Lee, P. Nikolaev, H. Dai, P. Petit, J. Robert, Ch. Xu, Y.H. Lee, S.G. Kim, A.G. Rinzler, D.T. Colbert, G. Scuseria, D. Tománek, J.E. Fischer, R.E. Smalley, Science 273 (1996) 483.
[30] B.G. Demczyk, Y.M. Wang, J. Cumings, M. Hetman, W. Han, A. Zettl, R.O. Ritchie, Mater. Sci. Eng. A 334 (2002) 173.
[31] W.X. Chen, J.Y. Lee, Zh. Liu, Carbon 41 (2003) 959.
[32] Z.P. Guo, Z.W. Zhao, H.K. Liu, S.X. Dou, Carbon 43 (2005) 1392.
[33] T. Ishihara, M. Nakasu, M. Yoshio, H. Nishiguchi, Y. Takita, J. Power Sources 146 (2005) 161.
[34] J. Shu, H. Li, R. Yang, Y. Shi, X. Huang, Electrochem. Commun. 8 (2006) 51.
[35] Y. Zhang, X.G. Zhang, H.L. Zhang, Z.G. Zhao, F. Li, C. Liu, H.M. Cheng, Electrochem. Acta 51 (2006) 4994.
[36] J.Y. Eom, J.W. Park, H.S. Kwon, S. Rajendran, J. Electrochem. Soc. 153 (2006) A1678.
[37] M.M.J. Treacy, T.W. Ebbesen, J.M. Gibson, Nature 381 (1996) 678.
[38] E.W. Wong, P.E. Sheehan, C.M. Lieber, Science 26 (1997) 1971–1975.
[39] A. Peigney, Ch. Laurent, E. Flahaut, R.R. Bacsa, A. Rousset, Carbon 39 (2001) 507–514.
[40] F. Salver-Disma, C. Lenain, B. Beaudoin, L. Aymard, J.-M. Tarascon, Solid State Ionics 98 (1997) 145.
[41] S.C. Tsang, Y.K. Chen, P. Harris, M. Green, Nature 372 (1994) 159.
[42] E. Frackowiak, S. Gautier, H. Gaucher, S. Bonnamy, F. Beguin, Carbon 37 (1999) 61–69.
[43] D. Aurbach, B. Markovsky, I. Weissman, E. Levi, Y. Ein-Eli, Electrochim. Acta 45 (1999) 67.
[44] M.K. Datta, P.N. Kumta, J. Power Sources 165 (2007) 368.
[45] A. Ulus, Yu. Rosenburg, L. Burnstein, E. Peled, J. Electrochem. Soc. 149 (2002) A635–A643.